

Bed topography and lubrication inferred from surface measurements on fast-flowing ice streams

THROSTUR THORSTEINSSON,^{1*} CHARLES F. RAYMOND,¹ G. HILMAR GUDMUNDSSON,²
ROBERT A. BINDSCHADLER,³ PAUL VORNBERGER,³ IAN JOUGHIN⁴

¹Department of Earth and Space Sciences, Box 351310, University of Washington, Seattle, Washington 98195-1310, U.S.A.

E-mail: throstur@turdus.net

²British Antarctic Survey, Natural Environment Research Council, Madingley Road, Cambridge CB3 0ET, England

³NASA Goddard Space Flight Center, Code 971, Greenbelt, Maryland 20771, U.S.A.

⁴Jet Propulsion Laboratory, California Institute of Technology, 4800 Oak Grove Drive, Pasadena, California 91109-8099, U.S.A.

ABSTRACT. Observations of surface elevation (s) and horizontal velocity components (u and v) are inverted to infer the topography (b) and lubrication (c) at the bed of an ice stream, based on a linearized perturbation theory of the transmission of flow disturbances through the ice thickness. Synthetic data are used to illustrate non-uniqueness in the inversion, but also demonstrate that effects of b and c can be separated when s , u and v are specified, even with added noise to simulate measurement errors. We have analyzed prominent short-horizontal-scale (~ 2 km) features in topography and velocity pattern in a local 64 km by 32 km area of the surface of Ice Stream E, West Antarctica. Our preferred interpretation of bed conditions beneath the most prominent features on the surface identifies a deep trough in the basal topography with low lubrication in the base of the trough.

1. INTRODUCTION

Changes in the resistance to motion of ice streams over their bases is a primary concern with regard to accelerated discharge of ice from the West Antarctic ice sheet (WAIS) and the resulting sea-level rise. The conditions at the base of ice streams are best examined directly with access by boreholes (Kamb, 2001). Densely spaced information along profile paths can also be found from remote sensing using seismic (Blankenship and others, 1987; Anandakrishnan and others, 1998) and radar (Bentley and others, 1998; Gades and others, 2000) data. Inversion of the disturbance of surface topography and velocity field arising from bumps and sticky spots on the bed provides another line of attack that has the potential to provide broad map-plane spatial coverage utilizing satellite remote sensing (MacAyeal and others, 1995). The spatial pattern is key to examining the relationship between basal topography and local lubrication, which is still unknown for any ice stream.

Small-scale undulations on the surface of ice streams and flow variations associated with them are pervasive and characteristic of streaming flow. An example of an ice-stream surface is shown in Figure 1. In this paper we use the theory of glacier flow perturbations caused by small variations in bed topography and/or basal lubrication (Gudmundsson, 2003) to investigate the sources of these surface features and their implication for basal conditions retarding ice-stream motion. The theory has been used to

show that flow stripes on ice streams can form from flow over localized bedrock bumps or sticky spots (Gudmundsson and others, 1998).

The goal of this paper is to use maps of the horizontal variation in x and y of surface elevation $s(x, y)$ and components of horizontal velocity $u(x, y)$ and $v(x, y)$ to infer bed elevation $b(x, y)$ and basal lubrication $c(x, y)$ under an ice stream where $c(x, y)$ relates motion tangential to the bed to the local shear stress. In principle, bed topography $b(x, y)$ could be measured with radio-echo sounding, which would allow a more constrained computation of lubrication $c(x, y)$ and a more secure examination of any correlation between b and c . In practice, map-plane measurements of b are not likely to be realized in the near future at a very fine spatial scale over large areas. For this reason we attempt to infer both b and c .

The primary assumption of the theory is that $b(x, y)$ and $c(x, y)$ disturbances to flow and associated topography are small compared to mean conditions, thus allowing analysis using perturbation theory (Hutter and others, 1981). In addition, the ice is assumed to be linearly viscous with an exponential vertical variation in viscosity, which can partly account for effects from vertical variation of temperature and non-linearity of the ice flow law.

The theory can be formulated in terms of transfer functions that relate bed topography, b , and basal lubrication, c , to surface topography, s , and velocity components, u , v and w (Gudmundsson, 2003). It is an extension of earlier work by Budd (1970), Hutter and others (1981), Hutter (1983), Whillans and Johnsen (1983), Balise and Raymond (1985), Reeh (1987) and Jóhannesson (1992) to include full three-dimensionality in the flow and time dependence in the basal boundary condition. The theory shows that effects on the

*Present address: Science Institute, University of Iceland, Sturlugata 7, IS-101, Reykjavík, Iceland.

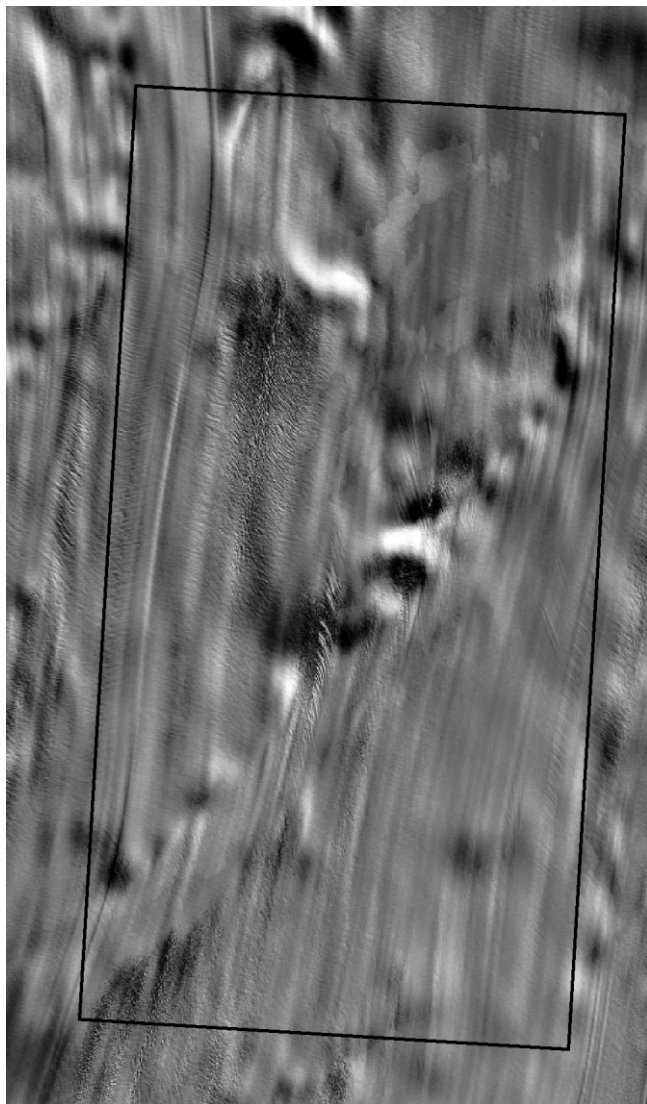


Fig. 1. Landsat image of a $64 \times 32 \text{ km}^2$ area on Ice Stream E, West Antarctica. Surface undulations of various wavelengths are made visible by oblique solar illumination from the top of the image. Direction of motion is westward, approximately from top to bottom of the figure. Coordinates of the corners of the outlined box are: lower left: 79.9890° S , 144.3307° W ; upper left: 79.6543° S , 140.6127° W ; upper right: 79.9958° S , 139.5263° W ; lower right: 80.3421° S , 143.3374° W .

ice flow from localized perturbations in the basal conditions (b or c) are strongly attenuated toward the surface. This attenuation complicates the inverse calculation of bed conditions from surface measurements (Bahr and others, 1994). The bed-to-surface attenuation is smaller when the mean basal motion is large compared to motion from internal deformation. Thus, ice streams that move dominantly by motion over their beds are amongst locations where this kind of inversion has some chance of success.

To test inversion procedures, we specify various patterns of $b(x, y)$ and $c(x, y)$ and generate corresponding synthetic data for $s(x, y)$, $u(x, y)$ and $v(x, y)$ with added noise to simulate errors. We find that successful inversion should be possible for a useful range of spatial scales in the fast-flowing ice streams.

Based on the experience gained from inversion of synthetic data, we investigate the covariation of b and c in a local area of Ice Stream E, West Antarctica, where measure-

ments of s , u and v are available. This area lies within a larger area examined earlier by MacAyeal and others (1995). Our analysis differs from theirs in several ways. The fully three-dimensional treatment of the flow enables us to probe for small-spatial-scale features that cannot be taken into account by the vertically integrated treatment used by MacAyeal and others (1995). We input detailed information on the surface topography derived from recent altimetry and photogrammetry (Bindschadler and others, 1996), whereas MacAyeal and others (1995) used only velocity pattern as input and inverted for the surface topography. We also use updated surface velocity measurements (Joughin and others, 1999). The main disadvantage of our perturbation-based method is that it is restricted to small variations from mean bed conditions, and boundary conditions on the edges of the domain cannot be arbitrarily specified. Thus, we cannot examine questions such as the relative role of side drag and longitudinal forces associated with large amplitude and spatial-scale variations in bed conditions; these questions are better attacked by the MacAyeal and others (1995) approach.

We have found that spatially correlated variations in basal topography and lubrication are required to explain the combined features of surface elevation and velocity in Ice Stream E.

2. DESCRIPTION OF THE FORWARD THEORY

The forward theory is described in detail by Gudmundsson (2003). It solves equations for creeping flow of an incompressible Newtonian fluid for deviations in velocity field and associated surface evolution from mean steady conditions as caused by small, possibly time-dependent changes in the basal topography and lubrication. In this paper, we assume time-independent basal conditions on a bed $z = b(x, y)$, where the vertical coordinate is z . The upper surface elevation is taken as $z = s(x, y)$. The fluid viscosity η is allowed to vary exponentially with depth $s - z$ beneath the surface given as

$$\eta(z) = \eta_s e^{-\mu(s-z)}, \tag{1}$$

where η_s is the viscosity at the upper surface and μ scales the vertical variation of viscosity.

Boundary conditions on the bed are specified by the equation:

$$\mathbf{u} = c(x, y)\mathbf{t} \cdot \mathbf{T}(\mathbf{n})\mathbf{t}, \tag{2}$$

where \mathbf{n} is the local normal to the bed, $\mathbf{T}(\mathbf{n})$ is the stress vector acting on the bed, and \mathbf{t} is the local tangent to the bed in the plane common to \mathbf{T} and \mathbf{n} . This proscribes no motion normal to the bed ($\mathbf{u} \cdot \mathbf{n} = 0$) and bed-tangential motion proportional to and in the direction of the local basal shear stress. The proportionality factor $c(x, y)$ describes the local lubrication of the bed. Corresponding boundary conditions on the upper surface $s(x, y)$ are no motion normal to the local surface and no shear stress tangential to it. Thus, accumulation, ablation and time evolution of the upper surface are not taken into account.

The bed height and its lubrication are partitioned as $b(x, y) = b_0(x, y) + b_1(x, y)$ and by $c(x, y) = c_0 + c_1(x, y)$. $b_0(x, y)$ is a mean bed represented by a plane of slope α_0 . We take the x axis to be down this slope, so $b_0(x, y) = b_0(x)$. c_0 is a constant mean lubrication. When b_1 and c_1 are zero and the ice thickness is uniform, the problem reduces to a uni-

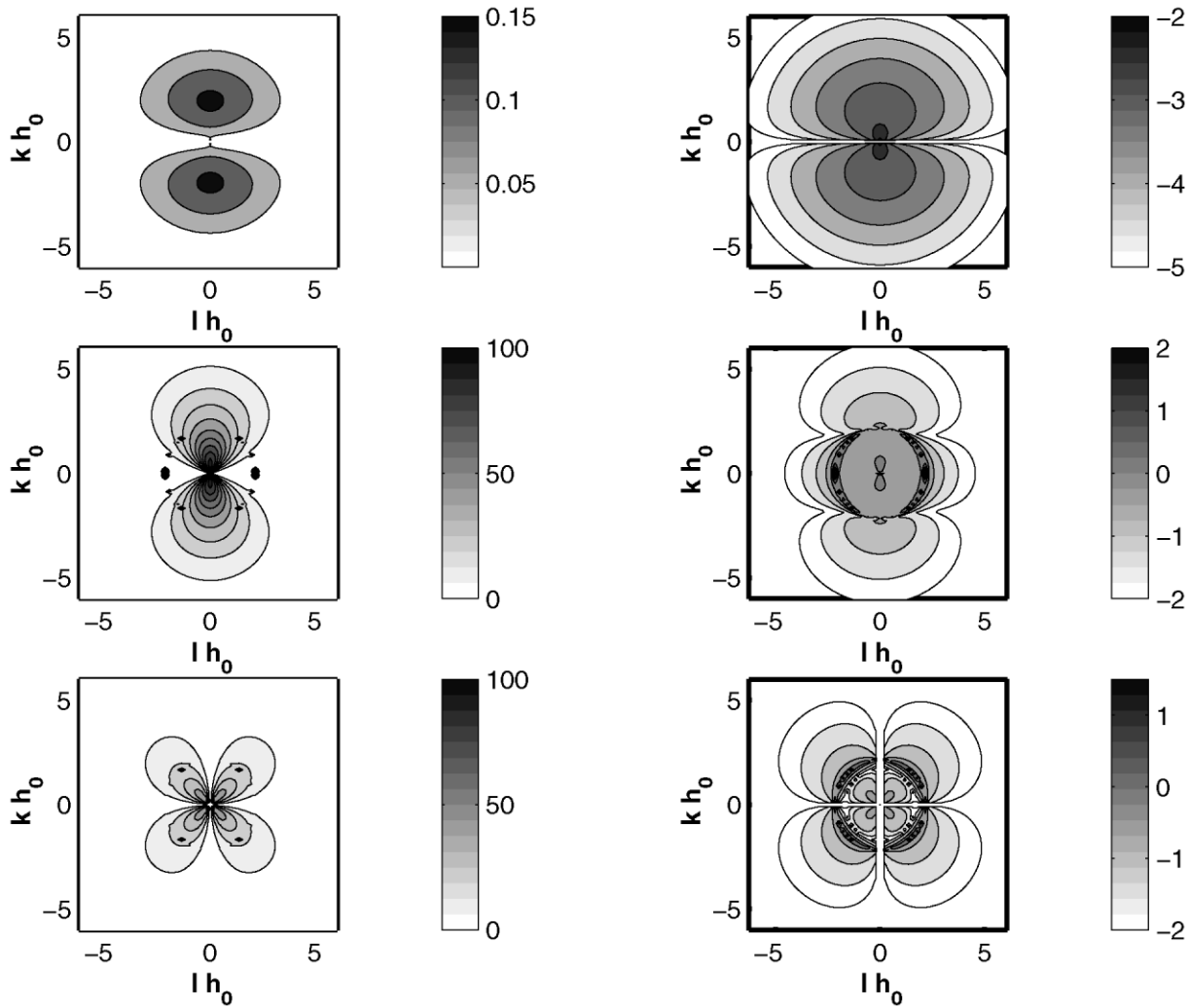


Fig. 2. The amplitude of the transfer functions \mathcal{T} as a function of longitudinal (k) and lateral (l) wavenumber for $\Omega = 10^2 \Xi = 2.5$, and $\alpha_0 = 0.11^\circ$. Left column: transfer function for bed topography B to surface topography S (\mathcal{T}_{SB}), longitudinal velocity U (\mathcal{T}_{UB}) and lateral velocity V (\mathcal{T}_{VB}). Right column: lubrication C to surface topography S (\mathcal{T}_{SC}), longitudinal velocity U (\mathcal{T}_{UC}) and lateral velocity V (\mathcal{T}_{VC}). Units in plots are: $[\mathcal{T}_{SB}] = 1$, $[\mathcal{T}_{UB}] = [\mathcal{T}_{VB}] = (u_0/h_0)$, $[\mathcal{T}_{SC}] = h_0/C$, $[\mathcal{T}_{UC}] = [\mathcal{T}_{VC}] = u_0/C$, where $[C] = u_0/(\rho g \alpha_0 h_0)$. Note that the grayscales are calibrated using \log_{10} for \mathcal{T}_{SC} , \mathcal{T}_{UC} and \mathcal{T}_{VC} and that $l = 0$ and $K \rightarrow 0$, $[\mathcal{T}_{SB}] \rightarrow 1$, although not seen on the grid here.

formly sloped slab that moves by shearing over its thickness at a rate

$$u_d = \frac{\rho_i g \alpha_0 h_0^2}{2\eta_s} \left[2 \frac{e^{\mu h_0} (\mu h_0 - 1) + 1}{(\mu h_0)^2} \right], \quad (3)$$

and moves uniformly over its bed at a rate

$$u_b = c_0 \rho_i g h_0 \alpha_0, \quad (4)$$

where $h_0 = s_0(x) - b_0(x)$ is the constant thickness of the slab. This solution is regarded as a mean reference condition defined by h_0 , α_0 , c_0 , η_s and μ . When $b_1 \ll h_0$ and $c_1 \ll c_0$ are specified, perturbation analysis of the full three-dimensional field equations for incompressible, creeping flow and the boundary conditions gives solutions for the full distributions of all components of velocity ($u_1(x, y, z)$, $v_1(x, y, z)$, $w_1(x, y, z)$) and strain rate, stress and the height of the surface ($s_1(x, y)$). Setting the perturbation equations in non-dimensional form (Gudmundsson, 2003) shows that the characteristics of the solutions are determined by three dimensionless parameters: the slope α_0 , a measure of the vertical variation of viscosity

$$\Xi \equiv \mu h_0, \quad (5)$$

and the slip ratio

$$\Omega \equiv \frac{u_b}{u_d} = \frac{c_0 \eta_s}{h_0} \left[\frac{e^\Xi (\Xi - 1) + 1}{\Xi^2} \right]^{-1}. \quad (6)$$

Definition of a mean reference condition in an actual ice stream is straightforward in principle. h_0 and α_0 can be found from sparse radio-echo sounding measurements and elevation models from satellite altimetry. In many WAIS ice streams, $u_d \ll u_b$, so c_0 can be estimated directly from the surface velocity. η_s and μ can be chosen to best match the vertical variation of effective viscosity associated with the non-linear ice-flow law for the mean flow and the temperature distribution. Ξ and Ω can be determined in a similar manner.

We focus on the connection of perturbations on the upper surface $s_1(x, y)$, $u_1(x, y, s)$ and $v_1(x, y, s)$, which are accessible to measurement, with those on the bed $b_1(x, y)$ and $c_1(x, y)$, which are not accessible to direct measurement. For notational compactness we drop the subscript 1, and $s(x, y)$, $u(x, y)$, $v(x, y)$, $b(x, y)$ and $c(x, y)$ will henceforth represent the perturbations.

Description of the general results and much of the appli-

cation of the theory is done in wavenumber space. Capital letters $S(k, l)$, $B(k, l)$, $C(k, l)$, $U(k, l)$ and $V(k, l)$ denote the Fourier transform \mathcal{F} of surface elevation $s(x, y)$, bed elevation $b(x, y)$, basal lubrication $c(x, y)$, longitudinal $u(x, y)$ and lateral $v(x, y)$ velocity, respectively. For example $\mathcal{F}[s(x, y)] = S(k, l)$, which we will write as S .

The solutions for surface topography S and velocity components U and V are then represented in wavenumber space as

$$S = T_{SB}B + T_{SC}C, \tag{7}$$

$$U = T_{UB}B + T_{UC}C, \tag{8}$$

$$V = T_{VB}B + T_{VC}C, \tag{9}$$

where the transfer functions \mathcal{T} depend on α_0 , Ξ and Ω . Figure 2 shows transfer functions as a function of longitudinal (k) and lateral (l) wavenumber for the case where $\alpha = 0.11^\circ$, $\Omega = 100$ and $\Xi = 2.5$, which are values appropriate for the case of Ice Stream E considered below. A number of narrow peaks can be seen for $k^2 + l^2 \approx 1$ in the velocity transfer functions (Fig. 2). These are presumably related to the introduction of numerical errors, as a 6×6 matrix must be inverted for each wavenumber to solve for integration constants entering the transfer function. A singular-value decomposition of this matrix shows that for certain combinations of wavenumbers, mean surface slope and vertical variation of viscosity, its singular values become small and the matrix almost singular. These spurious peaks are narrow and isolated, and although it is not clear why they appear, they do not affect the results of the inversion.

3. THE INVERSE PROBLEM

We use a least-squares inversion of Equations (7–9) to find B and C that give the best consistency with specified S , U and V . Error-weighted residuals are defined as

$$R_S = \frac{1}{\Sigma_S} (S - T_{SB}B - T_{SC}C), \tag{10}$$

$$R_U = \frac{1}{\Sigma_U} (U - T_{UB}B - T_{UC}C), \tag{11}$$

$$R_V = \frac{1}{\Sigma_V} (V - T_{VB}B - T_{VC}C), \tag{12}$$

where Σ_S , Σ_U and Σ_V are the rms observation errors for S , U and V , which are assumed to be independent. The error weightings non-dimensionalize the expected residual to about 1 in each case. Following Menke (1989) minimization of $R^2 \equiv (R_S^*R_S + R_U^*R_U + R_V^*R_V)$ gives

$$\mathbf{X} = (\mathbf{G}^H \mathbf{E} \mathbf{G})^{-1} \mathbf{G}^H \mathbf{E} \mathbf{Y}, \tag{13}$$

where

$$\mathbf{X} = \begin{bmatrix} B \\ C \end{bmatrix}, \mathbf{Y} = \begin{bmatrix} S \\ U \\ V \end{bmatrix}, \mathbf{G} = \begin{bmatrix} T_{SB} & T_{SC} \\ T_{UB} & T_{UC} \\ T_{VB} & T_{VC} \end{bmatrix}, \tag{14}$$

\mathbf{E} is an error matrix, here assumed to be diagonal with Σ_S^{-2} , Σ_U^{-2} , Σ_V^{-2} , along the diagonal, and superscript H denotes the Hermetian transpose,

$$\mathbf{G}^H = \begin{bmatrix} T_{SB}^* & T_{UB}^* & T_{VB}^* \\ T_{SC}^* & T_{UC}^* & T_{VC}^* \end{bmatrix}. \tag{15}$$

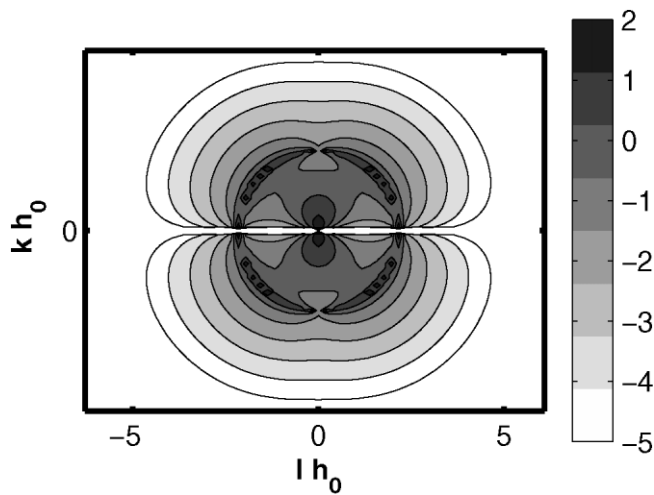


Fig. 3. $D(k, l)$ defined in Equation (19) for $\Omega = 10^2$, $\Xi = 2.5$ and $\alpha_0 = 0.11^\circ$ with $\Sigma_s = 2 \text{ m}$, $\Sigma_u = \Sigma_v = 5 \text{ m a}^{-1}$. The grayscale gives D in units of $\log_{10}(h_0 C)^{-2} = (\rho g \alpha_0 / h_0)^2$.

For compactness, we define

$$K = T_{SB}^* T_{SC} \Sigma^2 s + T_{UB}^* T_{UC} / \Sigma^2 u + T_{VB}^* T_{VC} / \Sigma^2 v,$$

$$L = T_{SB}^* T_{SB} \Sigma^2 s + T_{UB}^* T_{UB} / \Sigma^2 u + T_{VB}^* T_{VB} / \Sigma^2 v,$$

$$M = T_{SC}^* T_{SC} \Sigma^2 s + T_{UC}^* T_{UC} / \Sigma^2 u + T_{VC}^* T_{VC} / \Sigma^2 v,$$

$$Y_B = S T_{SB}^* \Sigma^2 s + U T_{UB}^* / \Sigma^2 u + V T_{VB}^* / \Sigma^2 v,$$

$$Y_C = S T_{SC}^* / \Sigma^2 s + U T_{UC}^* / \Sigma^2 u + V T_{VC}^* / \Sigma^2 v.$$

Then the solutions for the bed B and lubrication C are

$$B = (M Y_B - K Y_C) / D, \tag{17}$$

$$C = (-K^* Y_B - K Y_C) / D, \tag{18}$$

where

$$D = L M - K K^*. \tag{19}$$

The solution for B and C involves dividing by D , which is pictured in Figure 3. The inversion is problematic for those (k, l) where D is zero or small. This is the case for all large wavenumbers (wavelengths shorter than about $2h_0$) and $k = 0$ (some combinations of cross-flow variations in $b(\cdot, y)$ and $c(\cdot, y)$ which we will call longitudinal ridges and stripes). With regard to short-wavelength bed features, such fluctuations in the basal boundary condition will be accommodated by flow disturbances near the bed that do not influence the surface in a measurable way. It is interesting that longitudinal ridges and stripes are not transferred to the surface at all scales, and there will be a problem even for those inversion procedures that are concerned only with longer scale (e.g. MacAyeal and others, 1995). An easily understood example is indeterminacy of the combination of bed topography and slip condition across a valley glacier based on measurement of down-glacier velocity across its transversely flat upper surface. A shallower bed can be compensated by a more lubricated bed (or visa versa) to produce an equivalent fit to the down-valley speed on the surface. More generally, the problem is that lateral variations in b or c do not generate any change in surface topography or lateral velocity, and by arranging the phase and amplitude of b and c perturbations, the total surface velocity of the combination cancels. Then, there is no signal generated by b

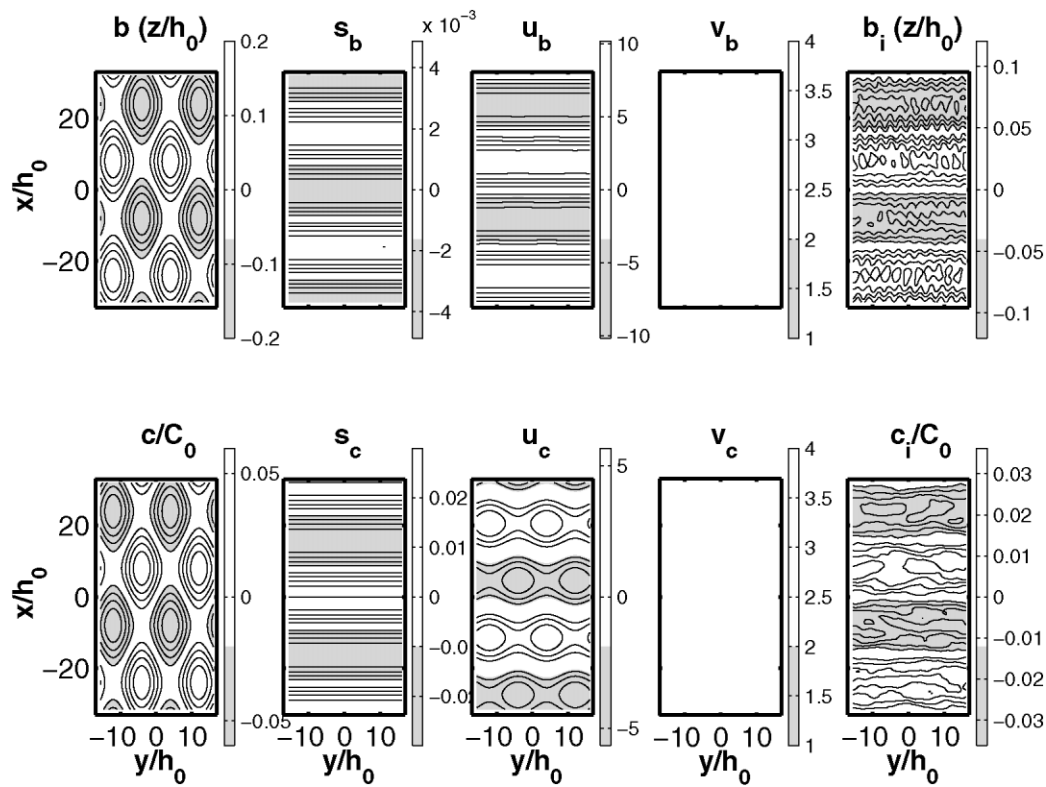


Fig. 4. Surface topography (s) and velocity (u and v) generated by superposition of longitudinal and lateral variations in b and c . The bed and lubrication patterns returned by the inversion of the surface “data”, added together in equal proportions with added noise in each signal (s , u and v) equal to 50% of its maximum amplitude, are shown on the far right as b_i and c_i .

and c at the surface at all. These kinds of bed features that do not transfer to the surface are in the null space of the forward problem. Such features can be added to any inversion for b and c without affecting the fit to surface data about s , u

and v . They display the non-uniqueness of the inversion. Correspondingly, it is not possible to invert for them on the basis of surface data.

To avoid this ill conditioning of the inverse, we use a

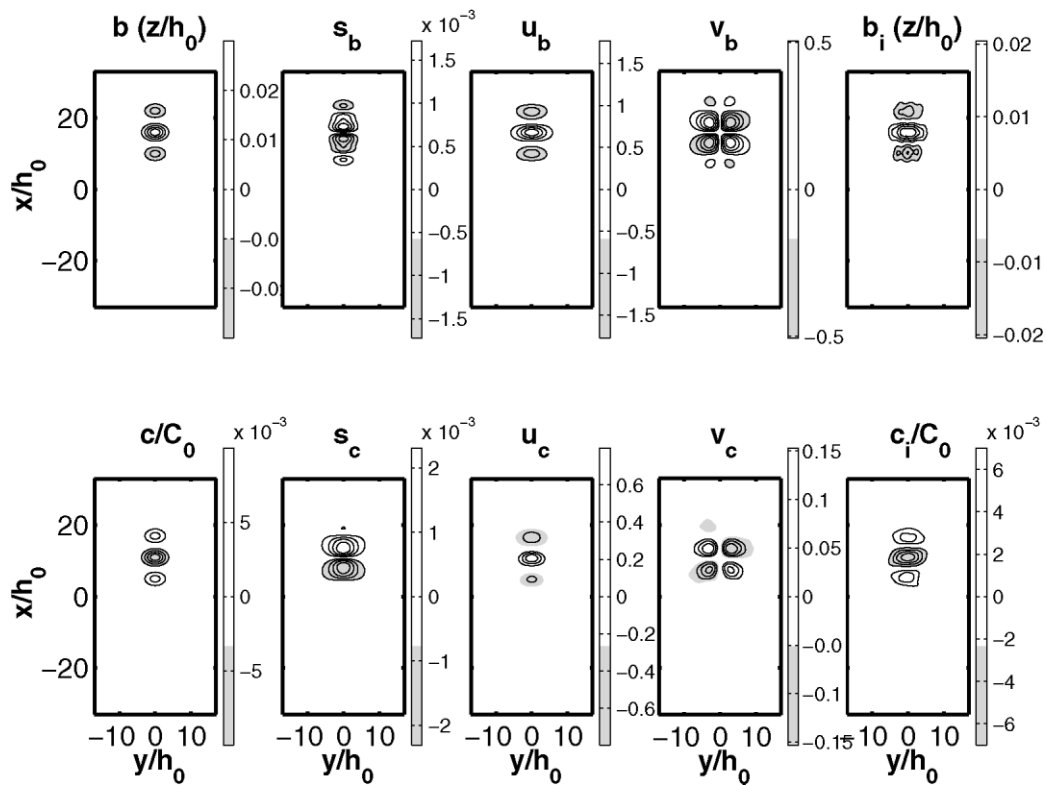


Fig. 5. Surface topography (s) and velocity (u and v) generated by Gaussian peak distributions for b and c . Note that the b and c patterns are slightly offset in the along-flow direction, and normalized to have a zero mean amplitude. The far right panels show the inferred bed and lubrication patterns, b_i and c_i , using the surface data in equal proportions, and adding noise that is 50% of the maximum amplitude of the signal (s , u and v).

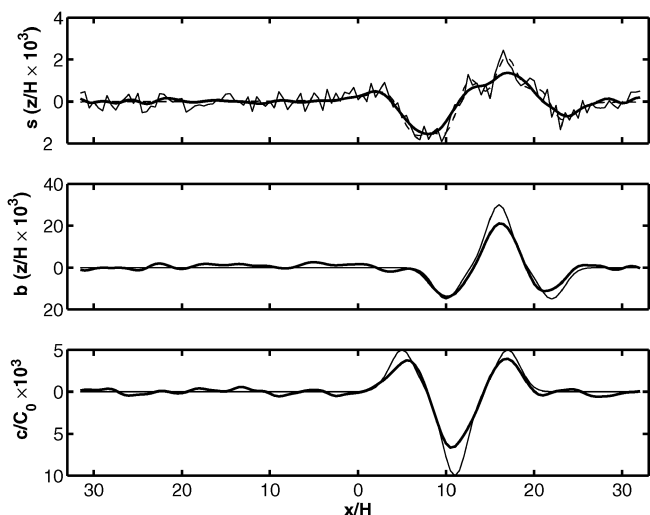


Fig. 6. Along-flow cross-section through $y = 0$ of the surface s , bed topography b and lubrication c , generated by the Gaussian bed and lubrication shown in Figure 5. The thin lines are the input. The dashed line in the top plot is the surface with added noise. The thick lines are the surface, bed elevation and lubrication inverted using the noise-degraded surface signals.

truncated version of D as a filter F to remove variations in the problematic wavenumber ranges from the input data S , U and V . The filter is

$$F = \begin{cases} D/P, & \text{if } D \leq P \\ 1, & \text{if } D > P. \end{cases} \quad (20)$$

It allows all wavelengths where D is larger than P to go through, but filters out other wavelengths. P is therefore an adjustable trade-off parameter. Smaller values of P give more detail, but may unjustifiably over-fit the surface data in view of errors. Larger values of P under-fit the data and may leave out features actually demanded by the data. We describe $P = \max(|D(k, l)|)\Omega^p$, where the power $p \leq 0$ is varied to adjust P .

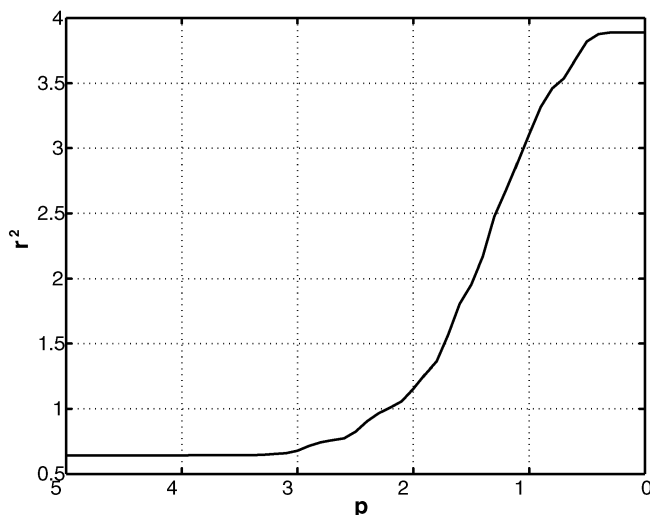


Fig. 8. Residual r^2 for inversion as a function of the power p in the filter defined by Equation (20) and following text.

Filtering is essential to avoid blow-up of errors in the data or the model, that could be interpreted erroneously as being generated by huge features on the bed. In practice, measurements of S , U and V may contain other noise that physically could have been generated from the bed and would not be removed by the filter F . In addition to measurement errors, such noise could arise from interference outside the model region transmitted or advected into it, for example flow stripes (Gudmundsson and others, 1998) or non-steady surface topography.

The capabilities and limitations of the inversion procedure can be explored using synthetic data. Our procedure is to use the forward theory (Equations (7–9)), to calculate s , u and v due to prescribed distributions of b and c . We combine the patterns generated by b and c and add random noise to each of the resulting total s , u and v signals. The noise amplitude is set at 50% of the maximum amplitude of each (combined) signal. This is similar to the noise level

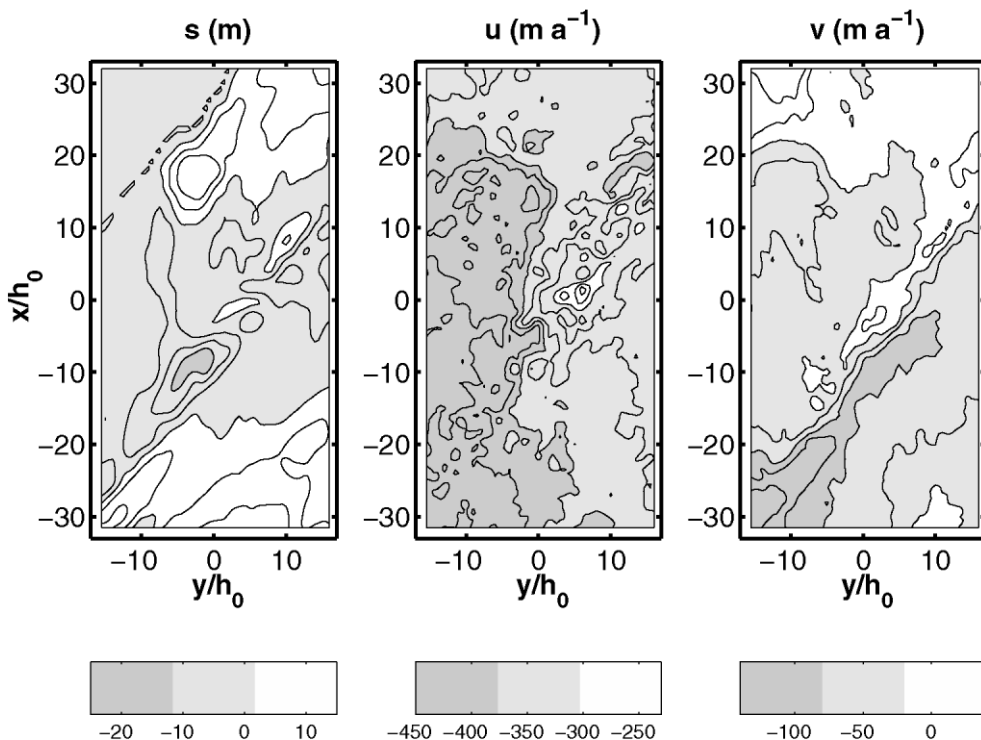


Fig. 7. Ice Stream E topography s , with the mean elevation and gradient removed, and velocity along flow (u) and lateral to flow (v).

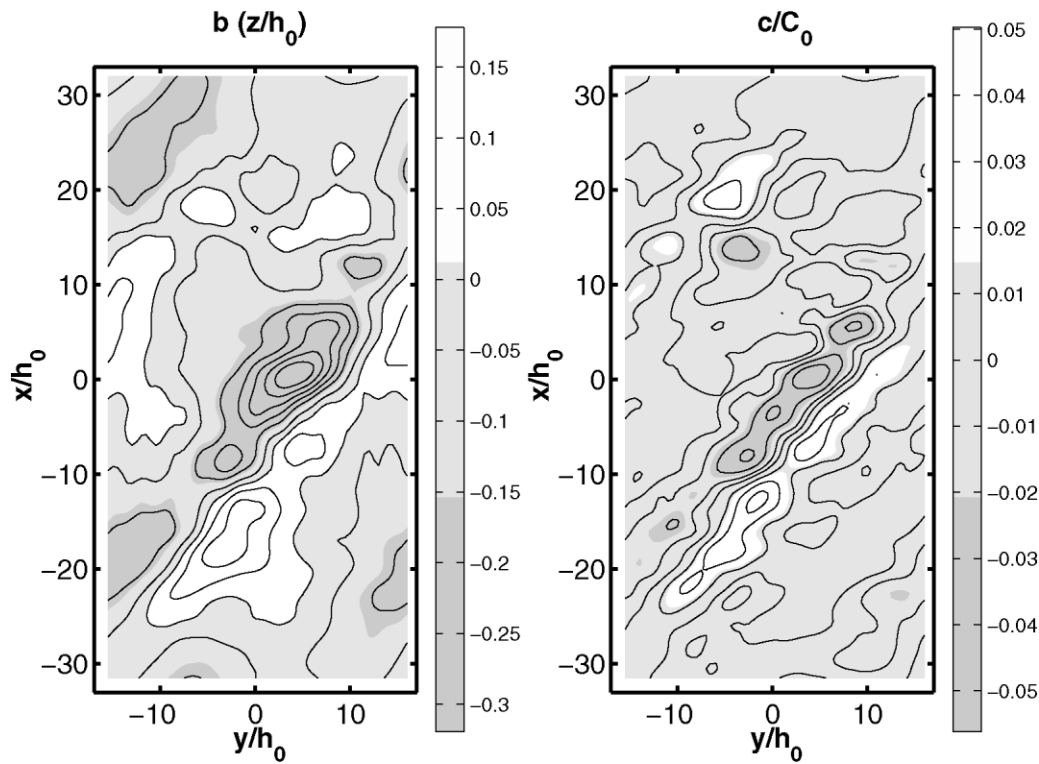


Fig. 9. Preferred inversion for b and c using s , u and v (Fig. 7) with $h_0 = 1100$ m, $\alpha_0 = 0.11^\circ$, $\Omega = 100$ and $\Xi = 2.5$.

in data from the surface of Ice Stream E that we examine below. We then invert for b and c using the combined s , u and v distributions with the added noise. A number of these synthetic inversions have been done. Only two examples are given here that illustrate the limitations and successes.

The checkerboard pattern shown in Figure 4 combines both lateral and longitudinal variations in b and c and provides an example where some information about the bed is transferred to the surface and some is not. The substantial lateral variation at the bed in both b and c appears on the surface only as a small lateral variation in u . Correspondingly, the inverted b_i and c_i (far right in Fig. 4) captures only the longitudinal variations. The filtering procedure (Equation (20)) suppresses production of large unrealistic lateral variations in b and c that would otherwise be generated by the noise. The small high-frequency lateral variations are a result of noise that has not been fully taken into account by the filtering. This example illustrates the unfortunate reality that the inversion is blind to certain features of b and c , but also demonstrates that the filtering stabilizes the inversion against the corresponding indeterminacy.

Gaussian shape perturbations in b and c provide an example of localized bed features with both longitudinal and lateral spatial variation. Figure 5 shows input and inverted b and c . Figure 6 shows a longitudinal section along $y = 0$. Remember that, in this and the previous example, the signals (s , u , v) generated by b and c are added together and degraded by noise before the inversion. This example shows that this inversion method can separate effects from b and c perturbations and accurately recover both longitudinal and lateral features of their spatial patterns including their relative positions.

4. Application to Ice Stream E

Figure 7 shows surface elevation $s(x, y)$ and velocity $u(x, y)$, $v(x, y)$ that have been extracted from satellite imagery of

Ice Stream E (Bindschadler and others, 1996) at locations covering the area shown by the box in Figure 1. We invert for the basal conditions within this box based on the data in Figure 7. All of s , u and v have a linear feature running from the lower left corner to the upper right corner. Most of our discussion will focus on the features at the bed that are responsible for these most prominent surface features.

At this location $h_0 = 1.1$ km and $\alpha_0 = 0.11^\circ$. The mean longitudinal speed is 370 m a⁻¹. There is a mean lateral shear strain rate of 0.04 a⁻¹. The deformational velocity u_d is estimated to be 5.4 m a⁻¹ using the standard temperature-dependent, non-linear flow law for ice (Paterson, 1994, p. 97). Temperature was estimated following the theory of Robin (1955), assuming steady state with a surface temperature of 247 K (Engelhardt and others, 1990), a bed temperature at the pressure-melting point, a surface accumulation rate of 0.1 m a⁻¹ and a linear vertical variation of vertical velocity. This estimate yields a temperature profile in reasonable agreement with temperature measured through Whillans Ice Stream (Engelhardt and others, 1990). The effect of the mean lateral shear strain rate on viscosity and an 18% reduction in the surface-parallel shear stress by side drag (Raymond, 2000) were taken into account. The implied dimensionless value for Ω is then $370/5.4 = 68$ (i.e. of order 10^{-2} which is the value used in the inversion described below). The effective viscosity decreases with depth beneath the surface in an approximately, although not exactly, exponential manner corresponding to dimensionless $\Xi = \mu h_0 = 2.5$. The value of U_d calculated as above is reproduced by Equation (5) with this value of μ and $\eta_s = 3.7 \times 10^{14}$ Pa s.

Since the transfer-function theory analysis in the wavenumber domain treats the boundaries as periodic, discontinuities are introduced at the boundaries, and the inversion will not be reliable near those boundaries. To alleviate this problem, we first linearly taper the data to zero over 10 km at up- and downstream edges and over 5 km on the sides. Then we remove the mean elevation and gradient (slope

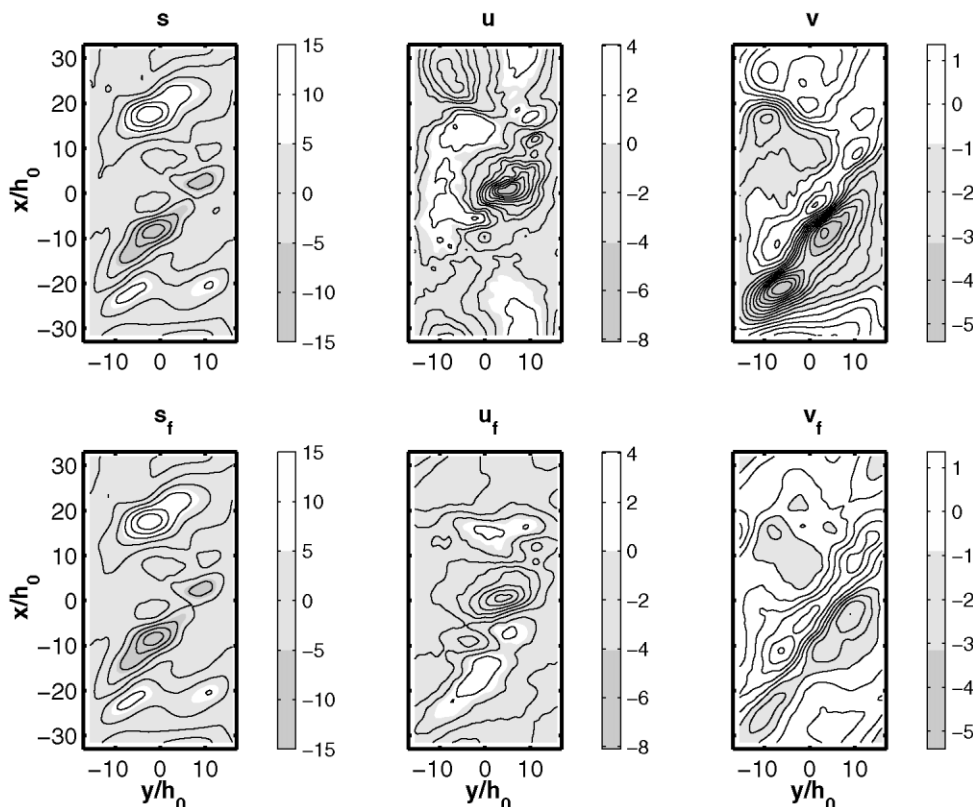


Fig. 10. Input data (Fig. 7 with gradients removed and filtered (Equation (20)). Bottom row shows s , u and v recovered by applying forward theory to b and c inferred from inversion (Fig. 9). The surface topography s is in m, and the velocities are in $m a^{-1}$.

α_0) from the surface topography data. We also remove the mean longitudinal velocity and the lateral velocity gradient from u .

Error levels (Equations (10–12)) are estimated to be $\Sigma_s = 2.2$ m, $\Sigma_u = 10$ $m a^{-1}$ and $\Sigma_v = 20$ $m a^{-1}$. Velocity data are from feature tracking, and errors are expected to be uncorrelated from one location to another independent of distance. Thus, we expect a flat error spectrum for u and v . On the other hand, s is determined by integration of slopes, which would produce a red error spectrum. We nevertheless use a flat error spectrum for s , since we are suppressing short-scale features on the surface in any case because of

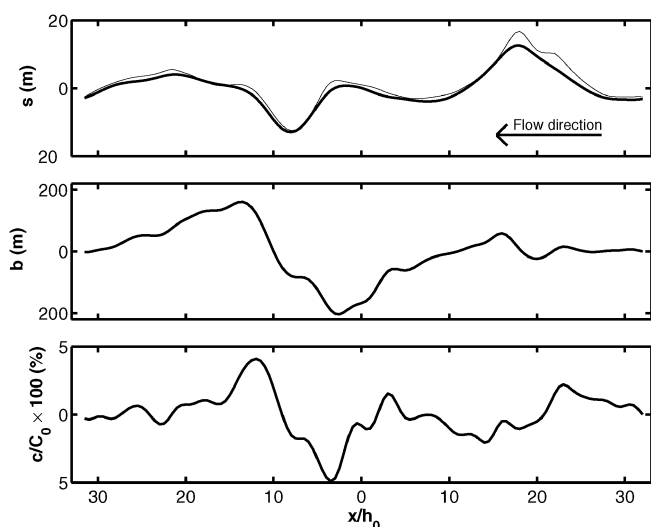


Fig. 11. Observed (thin line) and recovered (thick line) surface topography (s), bed topography (b), and lubrication (c/C_0) along $y = 0$.

the transfer characteristics. The error-weighted root-mean-square (rms) residual is $r^2 = (r_s^2 + r_u^2 + r_v^2)/3$. Here $r_x^2 = \Sigma_{i=1}^N (x_{measured} - x_{calculated})^2 / (N \Sigma_x^2)$, where N is the number of gridpoints and x stands for s , u or v .

Figure 8 shows the scaled residuals that result from the inversion for different cut-off for the filtering as described by P (Equation (20)). A value of $p = -2$ gives residuals at a level consistent with estimated errors and we use this value for our preferred inversion.

Figure 9 shows the inferred bed topography (b) and basal lubrication (c) using these data. The overall agreement is consistent with expected errors (Table 1, first row). The error-weighted rms residual is $r^2 = 0.404$. Table 1 shows the r_x values for each of the surface variables, using the error levels suggested above, $\Sigma_s = 2.2$ m, $\Sigma_u = 10$ $m a^{-1}$ and $\Sigma_v = 20$ $m a^{-1}$.

The main bed feature identified in the inversion is a prominent linear zone involving both $b(x, y)$ and $c(x, y)$ that runs diagonally across the region from $x/h_0 \sim -21$ on the left side ($y/h_0 \sim -15$) to $x/h_0 \sim 15$ on the right side ($y/h_0 \sim +15$). It is a deep trough in the topography and a low in the lubrication that approximately coincide. It lies

Table 1. The r_x and r^2 values for inversions for both b and c , only b or only c (see text)

	r_s	r_u	r_v	r^2
b and c	1.010	0.317	0.301	0.404
b only	1.016	0.431	0.436	0.469
c only	1.011	0.348	0.356	0.424

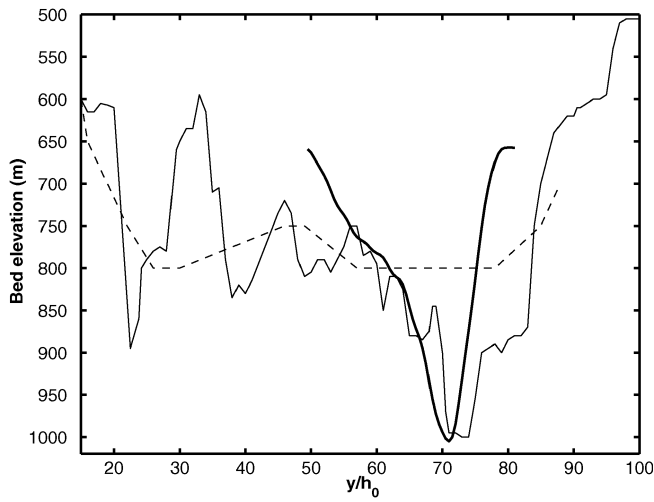


Fig. 12. Comparison of bed measured by radar as given by (Bindschadler and others (1996) (thin line), the inversion by (MacAyeal and others (1995) (dashed line) and the inferred bed (thick line) near $x/h_0 = 2.5$.

slightly upflow from the linear surface feature in s , u and v apparent in Figure 7.

Outside of this linear zone, there also appears to be a correlation between lows in the topography and lows in lubrication. However, that correlation is less compelling, especially recognizing that the inversion is less reliable near the boundaries of the solution region.

Figure 10 compares the observed (top row) and recovered (bottom row) surface topography (s) and velocity components (u , v). The spatial patterns are consistent. The amplitudes are recovered less well, especially for u and v . Figure 11 (top panel) gives a more detailed comparison of observed and recovered surface topography (s) along flow through the center of the solution region ($y/h_0 = 0$). The bottom panels of Figure 11 show the inferred bed topography (b) and lubrication (c) along the same line. The trough feature (Fig. 9, left panel) is displayed in diagonal section.

Figure 12 shows a transverse profile of the bed at $x/h_0 \sim 2.5$. This is aligned with a radar profile giving a measured bed topography (Bindschadler and others, 1996, fig. 10b) plotted here as a thin solid curve. The dashed curve in Figure 12 also shows the bed deduced by MacAyeal and others (1995, Fig. 6) for comparison. Neither inversion agrees completely with the radar measurements. The MacAyeal inversion gives a smoothed picture of the bed as it was designed to do. This inversion (thick solid line), following its design, captures more detail. It succeeds in identifying the deep, narrow trough evident in radar data, but there is an offset. Edge effects in the inversion may explain some of the offset. Co-

Table 2. The r^2 values for various combinations of Ω and Ξ , but fixed $\Sigma\dot{s}$ (see text)

Ξ	Ω					
	10	50	10^2	10^3	5	10^4
0	–	1.402	0.426	1.049	–	–
2.5	1.121	0.462	0.404	0.430	–	1.443
5	–	8.070	0.552	0.420	0.572	–
8	–	–	2.287	0.462	0.465	0.526

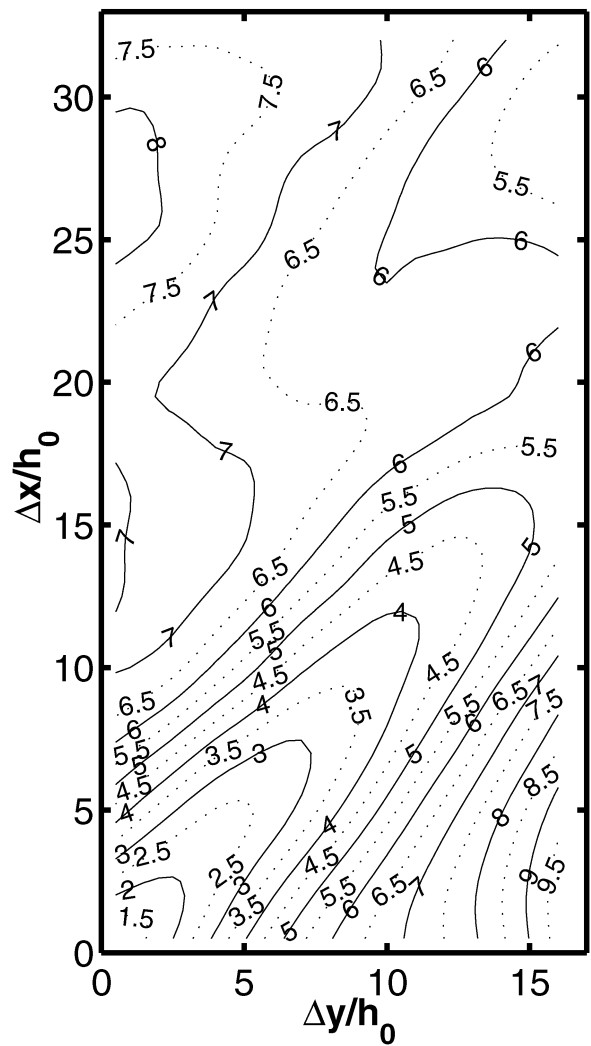


Fig. 13. Sensitivity of the weighted residual r^2 to shifts in the $c(x,y)$ pattern relative to $b(x,y)$ by Δx and Δy .

gistration errors in aligning the radar profile relative to the data for s , u and v may also contribute. However, the disagreement could arise because of nonuniqueness in the inversions discussed in section 3. Indeed, if the bed trough were aligned with the flow direction, it would produce a very small (or possibly zero) surface effect and would not be detectable with measurements of s , u and v .

Now we investigate how trustworthy this inversion is. We first examine sensitivity of the inversion to changes in Ω and Ξ (Table 2). It is encouraging that the best fits to the data are possible for combinations of Ω and Ξ that are close to the a priori values of 2.5 and 10^2 estimated as described above. That suggests the underlying physics of the model is reasonable. It also suggests that one might actually invert for Ω and Ξ . However, it is clear that the minimum in residuals is quite broad, and difficult to identify precisely. Inversions for different pairs of Ω and Ξ predict similar spatial features for b and c , but different amplitudes (higher amplitude on the bed as Ξ increases) and short scale variations (higher frequency on the bed if Ω increases). Therefore, if Ξ and Ω are not known, this inversion technique can retrieve the pattern of b and c but not the amplitudes.

Inversion for only the bed topography b or only basal lubrication c does not yield results as good as the combination (Table 1). The r^2 values for b and c alone are nevertheless still reasonable, and we cannot reject the corresponding inversions on this basis alone. The inversion for b only yields

larger peaks on the bed to produce the high in the surface topography (near $x/h_0 = 20$), and downstream the topography looks more like the c pattern from the b and c inversion. The c -only pattern stays similar to the c pattern from the inversion for both b and c , although not with as strong a ridge-like feature, and added slippery and sticky spots to create the topography high near $x/h_0 = 20$. However, our a priori expectation is that there are both b and c variations under the ice stream, and on this basis we prefer the combined b and c inversion result.

We now examine whether the correlation between the low in the topography and low in lubrication is a robust feature of the inversion under the supposition that spatial variation of both b and c is present. Figure 13 shows that the residual r^2 increases substantially when the $c(x, y)$ pattern is shifted by small $\Delta x/h_0$ and $\Delta y/h_0$ relative to the $b(x, y)$ pattern, especially for shifts that are perpendicular to the lineations. Reversing the sign of the lubrication or topography also produces clear disagreement with the surface data. If perturbations in b and c are both present, then the lows in b and c are evidently nearly coincident.

The existence of low lubrication (stickiness) in the bed trough can have two basic sources: (1) a distinctive bed morphologically such as a rough, hard rock or consolidated sediments, or (2) low water pressure resulting in relatively high effective normal stress. There are several factors that argue against (2). A trough should be a location of relatively low upward conduction of heat through the thick, overlying ice. There should be relatively high basal heat generation from friction where the bed is sticky. These factors would combine to produce higher basal melt rate in a sticky trough relative to its surroundings. The hydraulic gradient required to evacuate the extra meltwater would tend to produce high water pressure and low effective normal stress. The density difference between ice and water would also promote low effective normal stress in the trough. Finally, the bed low would tend to be a preferred flow path for water coming from upstream. These hydraulic effects associated with the low bed would tend to enhance lubrication. Therefore, we suggest that the first of the above explanations for low lubrication in the trough is more likely. We leave open the interesting question of why this sticky trough is there.

5. CONCLUSIONS

It is possible to invert measurements of surface topography and velocity for some features of bed topography and lubrication. Short-wavelength features ($\lambda \approx 2h_0$) and longitudinal ridges/troughs and stripes in lubrication at all lateral scales cannot be recovered, leading to intrinsic non-uniqueness in the inversion even with precise input data. Application of the inversion method to available observation on parts of the surface of Ice Stream E identifies a lineation on the bed of the ice stream that runs diagonally across the flow direction. While the available surface data allow the possibility that the basal lineation is a topographic trough with no variation of lubrication or that it is a low-lubrication (sticky) zone with no topography, our preferred interpretation is a topographic trough with low lubrication in its base.

ACKNOWLEDGEMENTS

We wish to thank T. Jóhannesson who provided valuable guidance and suggestions as Scientific Editor, and reviewers R. Greve and T. Payne for their constructive comments. This work was supported by U.S. National Science Foundation grant No. OPP-9526707.

REFERENCES

- Anandkrishnan, S., D. D. Blankenship, R. B. Alley and P. L. Stoffa. 1998. Influence of subglacial geology on the position of a West Antarctic ice stream from seismic observations. *Nature*, **394**(6688), 62–65.
- Bahr, D. B., W. T. Pfeffer and M. F. Meier. 1994. Theoretical limitations to englacial velocity calculations. *J. Glaciol.*, **40**(136), 509–518.
- Balise, M. J. and C. F. Raymond. 1985. Transfer of basal sliding variations to the surface of a linearly viscous glacier. *J. Glaciol.*, **31**(109), 308–318.
- Bentley, C. R., N. Lord and C. Liu. 1998. Radar reflections reveal a wet bed beneath stagnant Ice Stream C and a frozen bed beneath ridge BC, West Antarctica. *J. Glaciol.*, **44**(146), 149–156.
- Bindschadler, R., P. Vornberger, D. Blankenship, T. Scambos and R. Jacobel. 1996. Surface velocity and mass balance of Ice Streams D and E, West Antarctica. *J. Glaciol.*, **42**(142), 461–475.
- Blankenship, D. D., C. R. Bentley, S. T. Rooney and R. B. Alley. 1987. Till beneath Ice Stream B. I. Properties derived from seismic travel times. *J. Geophys. Res.*, **92**(B9), 8903–8911.
- Budd, W. F. 1970. Ice flow over bedrock perturbations. *J. Glaciol.*, **9**(55), 29–48.
- Engelhardt, H., N. Humphrey, B. Kamb and M. Fahnestock. 1990. Physical conditions at the base of a fast moving Antarctic ice-stream. *Science*, **248**(4951), 57–59.
- Gades, A. M., C. F. Raymond, H. Conway and R. W. Jacobel. 2000. Bed properties of Siple Dome and adjacent ice streams, West Antarctica, inferred from radio-echo sounding measurements. *J. Glaciol.*, **46**(152), 88–94.
- Gudmundsson, G. H. 2003. Transmission of basal variability to a glacier surface. *J. Geophys. Res.*, **108**(B5), 2253. (10.1029/2002JB0022107)
- Gudmundsson, G. H., C. F. Raymond and R. Bindschadler. 1998. The origin and longevity of flow stripes on Antarctic ice streams. *Ann. Glaciol.*, **27**, 145–152.
- Hutter, K. 1983. Theoretical glaciology; material science of ice and the mechanics of glaciers and ice sheets. Dordrecht, etc., D. Reidel Publishing Co.; Tokyo, Terra Scientific Publishing Co.
- Hutter, K., F. Legerer and U. Spring. 1981. First-order stresses and deformations in glaciers and ice sheets. *J. Glaciol.*, **27**(96), 227–270.
- Jóhannesson, T. 1992. Landscape of temperate ice caps. (Ph.D. thesis, University of Washington.)
- Joughin, I. and 7 others. 1999. Tributaries of West Antarctic ice streams revealed by RADARSAT interferometry. *Science*, **286**(5438), 283–286.
- Kamb, B. 2001. Basal zone of the West Antarctic ice streams and its role in lubrication of their rapid motion. In Alley, R. B. and R. A. Bindschadler, eds. *The West Antarctic ice sheet: behavior and environment*. Washington, DC, American Geophysical Union, 157–199. (Antarctic Research Series 77.)
- MacAyeal, D. R., R. A. Bindschadler and T. A. Scambos. 1995. Basal friction of Ice Stream E, West Antarctica. *J. Glaciol.*, **41**(138), 247–262.
- Menke, W. 1989. *Geophysical data analysis: discrete inverse theory. Revised edition*. New York, etc., Academic Press.
- Paterson, W. S. B. 1994. *The physics of glaciers. Third edition*. Oxford, etc., Elsevier.
- Raymond, C. F. 2000. Energy balance of ice streams. *J. Glaciol.*, **46**(155), 665–674.
- Reeh, N. 1987. Steady-state three-dimensional ice flow over an undulating base: first-order theory with linear ice rheology. *J. Glaciol.*, **33**(114), 177–185.
- Robin, G. de Q. 1955. Ice movement and temperature distribution in glaciers and ice sheets. *J. Glaciol.*, **2**(18), 523–532.
- Whillans, I. M. and S. J. Johnsen. 1983. Longitudinal variations in glacial flow: theory and test using data from the Byrd Station strain network, Antarctica. *J. Glaciol.*, **29**(101), 78–97.